JAAS

Dynamic characteristics of multi-charged ions emitted from nanosecond laser produced molybdenum plasmas

Journal:	*Journal of Analytical Atomic Spectrometry*
Manuscript ID	JA-ART-12-2019-000411.R1
Article Type:	Paper
Date Submitted by the Author:	15-Feb-2020

Complete List of Authors:	Wu, Ding; Dalian University of Technology School of Physics, School of Physics; Lawrence Berkeley National Laboratory Mao, Xianglei; Lawrence Berkeley National Laboratory, Chan , George; Lawrence Berkeley National Laboratory Russo, R; Lawrence Berkeley National Lab, Zorba, Vassilia; LBNL, ETA Ding, Hongbin; Dalian University of Technology, School of Physics

ARTICLE

Dynamic characteristics of multi-charged ions emitted from nanosecond laser produced molybdenum plasmas

Received 00th January 20xx,
Accepted 00th January 20xx

DOI: 10.1039/x0xx00000x

Ding Wu[a,b], Xianglei Mao[b], George C.-Y. Chan[b], Richard E. Russo[b], Vassilia Zorba[b,c*1], Hongbin Ding[a*2]

Diagnostics of plasma-wall interaction processes provide important information for nuclear fusion devices. Elucidation of the charge state distribution and temporal evolution of the multi-charged ions is essential to improve laser ablation-based diagnostics of the plasma-wall interaction processes. Molybdenum is a material of interest in fusion and has been used as the plasma-facing material of the first wall in the EAST tokamak. In this work, the dynamic characteristics of multi-charged ions emitted from a molybdenum plasma produced by a Q-switched Nd:YAG nanosecond laser (wavelength 1064 nm, pulse width 7 ns) were studied using time of flight mass spectroscopy under a pressure of 6×10^{-4} Pa. The charge state distribution and temporal evolution of the multi-charged ions at various laser power densities from 0.85 GW/cm^2 to 7.9 GW/cm^2 were systematically investigated. This power density range is commensurate to that used in LIBS and LIAS diagnostics of the plasma-wall interaction process in EAST tokamaks.The ion charge state was found to increase with laser power density and the observed maximum charge state was up to seven at the highest laser power density used in these experiments. The higher charged ions had greater velocities indicating that separation took place between the different charged ions during the plasma expansion process. The origin of multi-charged ions is attributed to step-wise ionization due to plasma shielding from strong laser absorption in the plasma and the reduction of the ablation rate with increase in laser power density. The velocities between these multi-charged ions were related to the acceleration of the transient plasma sheath during the laser interaction with the target and plasma.

1. Introduction

Laser ablation and plasma formation with subsequent particle and optical emission have been explored in many applications such as pulsed laser deposition (PLD) [1], laser ion sources [2], laser ignition [3], laser propulsion [4], laser inertial fusion [5], and extreme ultraviolet (EUV) lithography [6, 7]. Laser ablation-based spectroscopic techniques like laser-induced breakdown spectroscopy (LIBS) [8], laser ablation molecular isotopic spectrometry (LAMIS) [9-11], laser ablation inductively coupled plasma mass spectrometry (LA-ICP-MS) [12, 13] also have been developed for many chemical analysis applications. Although there is a large number of applications, a fundamental understanding of laser ablation mechanisms remains unknown. Laser ablation is a dynamic non-linear process that includes laser absorption by the target, thermodynamics (heating, phase transitions, cooling), plasma physics (collisions, nonlinear interactions), laser-plasma interaction, and gas dynamics (plasma expansion into vacuum or background gas) [8, 14-17]. The fundamental processes of laser ablation are important to understand for further improvement of many of these applications.

Multiply charged ions have not received much attention for chemical analysis applications (e.g., LIBS) because a reduced-pressure environment is required for their observation [18-24]. Many emission lines from multiply charged ions are in the vacuum ultraviolet (VUV) region which would require the use of specialized spectrometers. Also, multiply charged ions appear only during the very early phase of plasma expansion immediately following the laser pulse in which strong continuum emission is present. As such, multiply charged ions under atmospheric pressure in LIBS applications are not measured. LIBS has been applied under vacuum conditions for remote, in-situ, online monitoring of the plasma wall interaction (PWI) process such as erosion/deposition processes and retention of plasma fuel on the first walls of the Experimental Advanced Superconducting Tokamak (EAST) [25, 26], and also for analysis of the limiter tiles in the Wendelstein 7-X stellarator (W 7-X)[27]. Another laser-based technique named laser-induced ablation spectroscopy (LIAS) is also an important application for in-situ characterization of the first wall of nuclear fusion devices, which is based on the reaction between laser-induced plasma and ambient deuterium plasma[28-31]. As the Tokamak is operated in vacuum condition, understanding behaviors of multiply charged ions in laser induced plasma under vacuum can provide the necessary background information for evaluation on the use the emission lines from multiply charged ions for chemical analysis under vacuum environment. Further, through ion-electron recombination, a multiply charged ion is a source for the more commonly probed singly charge ion and neutral atom. Therefore, understanding the

[a.] School of Physics, Dalian University of Technology, Dalian 116024, PR China
[b.] Lawrence Berkeley National Laboratory, Berkeley, CA 94720, USA
[c.] Department of Mechanical Engineering, University of California, Berkeley, CA 94720, USA
*[1]Corresponding author: vzorba@lbl.gov
*[2]Corresponding author: hding@dlut.edu.cn

dynamics of multiply charged ions in laser induced plasma helps to better comprehend spectral and plasma information in vacuum condition.

Quantitative analysis using LIBS in the vacuum tokamak is challenging. Considering the rapid variation of the surface composition of the walls and harsh condition during the tokamak running period, calibration-free (CF) or CF-based methods would be more suitable for chemical analysis than using calibration standards. CF-based methods applied in air have been reported in many studies [32-37] and quantitative results are quite attractive. In vacuum, CF and CF-based methods also have been used in the analysis of hydrogen, deuterium, carbon, aluminum, tungsten etc. on the International Thermonuclear Experimental Reactor (ITER)-like plasma-facing materials (PFMs) in labs [34, 38-40]. Quantitative results should be reconsidered due to two important factors that were ignored including mass separation and multi-charged ions. In vacuum the mass effect of high and low Z elements leading to the space separation in laser produced plasma was confirmed [41, 42], which means that the relative concentration of different elements are inhomogeneous in the plasma. Therefore, LIBS quantitative analysis at a single location in the plasma may not be representative of the chemical composition of the sample. Moreover, the existence of multi-charged ions in the laser produced plasma also should be considered as their concentrations are quite abundant [21-23, 43]. The existence of multi-charged ions in laser produced plasma previously were not considered in CF and CF-based methods in vacuum, probably because the optical emission for multi-charged ions in the UV/EUV range [44] was beyond the operation range of the spectrograph. Multi-charged ions in the laser produced plasma in low pressure should be considered to develop better CF models and for accurate quantitative analysis of LIBS. Hence, the experimental measurements of the multi-charged ions during plasma expansion are needed to improve the CF models for better utilizing LIBS technique for the diagnosis of PWI process in vacuum tokamaks. Moreover, the investigation of evaporation, plume expansion, and particle emission processes also benefit better understanding of wall erosion and impurity transport under extreme conditions like plasma disruptions in tokamak.

We studied the dynamics of multi-charged ions emitted from a molybdenum plasma produced by ns-laser ablation using time of flight mass spectroscopy. A molybdenum (Mo) target was used as it is the main PFM of the first wall in the EAST tokamak due to properties such as high melting point, high thermal conductivity, low erosion rate, and low tritium retention[45]. The charge state distribution and temporal evolution of multi-charged Mo ions at various laser power densities were systematically investigated. The velocity distribution at various energy power densities also was measured.

2. Experimental set-up

Orthogonal-acceleration time-of-flight mass spectrometry was used to measure the ions generated in the laser produced plasma during ablation under vacuum (Fig.1). The fundamental properties of time-of-flight mass spectrometry and a detailed description of this setup can be found in Refs [46] and [47], respectively. A Q-switched Nd:YAG laser operating at its fundamental wavelength of 1064 nm was used to generate laser pulses with a 7 ns duration. The laser beam was focused through a plano-convex fused silica lens onto the molybdenum target (10 mm in diameter, 2 mm in thickness, >99.95% purity) placed between two repeller plates. The gap between the repellers is 1.5 cm. A high-speed photodiode (Thorlabs, DET10A) was used to monitor the laser pulses, and laser pulse energy was about 42 mJ focused onto the target. The pressure of the chamber was 6×10^{-4} Pa. Ions produced from laser ablation were accelerated by an extraction field (pulsed electric field) on the two repeller plates which was controlled by two high voltage MOSFET push-pull switches (Behlke, HTS 31-GSM). A 1.5 mm diameter hole in the one of the repeller plates allowed ions to be extracted 2.0 cm away from the sample surface. The distance from the ablation location to the negative repeller is about 1 cm. Hence, the ion collection is at about 26 degrees with respect to the target normal. It has been well-documented that the ion emission from a laser-produced plasma is having an angular distribution where higher charge states provide narrower distribution[48, 49]. And the ion collection angle highly influences the signal intensity, especially for the relative ratio which has not been considered in present work. After extraction, the ions drifted through the field free region and were reflected by a reflectron towards a micro-channel plate detector. A digital delay generator (Stanford Research Systems, DG645) was used to control the laser Q-switch and to trigger the high-voltage switches of the repellers. An oscilloscope (Tektronix, DPO3054) recorded the signal at the microchannel plate after the trigger.

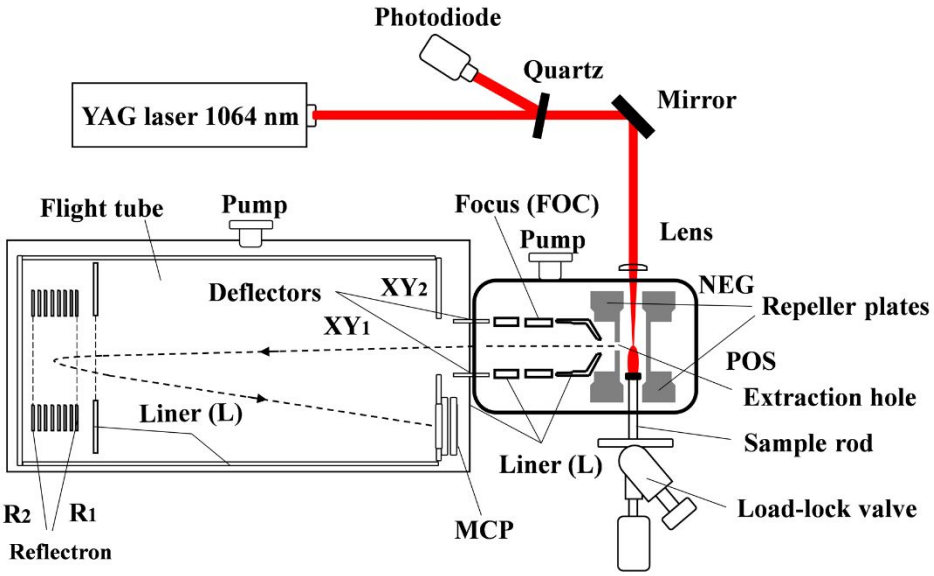

Fig.1 Schematic illustration of laser ablation in time of flight mass spectrometer

The timing diagram is shown in Fig.2. t_0 is the time of the laser pulse generation, t_d is the delay time relative to the laser pulse t_0, t_w is the time width of applied voltage on the repellers and t_{tri} is the time to trigger the oscilloscope to record the signals. By adjusting the delay time t_d relative to the laser pulse t_0, the temporal evolution of the plume could be investigated. The delay time range was t_d = 0.0-15.0 μs and the pulse voltage-width was fixed to t_w = 0.3 μs. The response time (from the trigger signal to the real switch time) of the two push-pull switches was measured and calibrated before the experiment to ensure accuracy of the delay time t_d. The measured response times of the negative and positive switches were about 170 ns and 140ns, respectively.

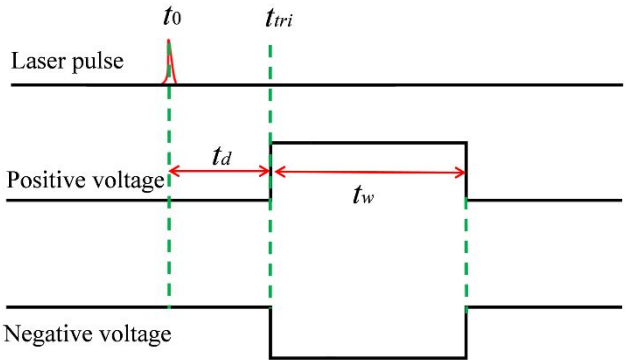

Fig.2 Timing sequence diagram of the laser and applied pulsed voltage, t_d = 0.0-15.0 μs, t_w = 0.3 μs

The power supply parameters are shown in Table 1. The laser ablation crater diameter was measured to be approximately 0.31 mm by an optical microscope as shown in Fig.3(a). Fig.3 (b) shows the cross-section depth profile which was measured using a White Light Interferometer. The maximum laser power density was estimated as 7.9 GW/cm^2. Neutral density filters (Thorlabs, absorptive ND series) were used to change the laser power density from 0.85 GW/cm^2 to 7.9 GW/cm^2. For each experiment, the first 30 shots were used to clean the Mo surface. Thereafter, mass spectra were collected by a single laser shot and the experiments were repeated five times to calculate the experimental error.

Table.1 Power supply parameters applied in TOF setup

Item	Voltage (V)
POS	+2913
NEG	0
Liner	-1500
XY_1	-268
XY_2	-10
R_1	-1500
R_2	4500
FOC	-9
MCP	-1400

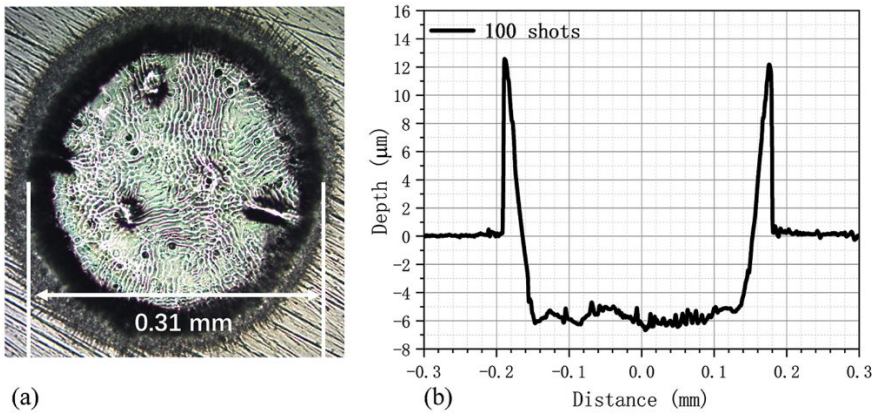

Fig.3 Photograph of the crater (a) and depth profile (b) after laser ablation in the Mo target with 100 laser shots, laser

power density 7.9 GW/cm^2.

3. Results and discussion

3.1 Time-resolved mass spectroscopy of multi-charged ions distribution

Figure 4 shows the time of flight response of Mo ions at various delay times with a gate width t_w of 0.3 μs, and laser power density of 7.9 GW/cm^2. Multi-charged molybdenum ions were observed and the maximum charge state was up to seven. No ions were observed at 0.10 μs due to the time needed for the ions to expand through the extraction hole at the vertical distance of 2.0 cm from the target surface. At delay times of 0.20 μs and longer, highly charged ions (Mo^{4+}, Mo^{5+}, Mo^{6+}, Mo^{7+}) were predominant and lower ionized Mo ions gradually appeared. The number of higher charged ions decreased with time. It has been proposed that the multi-charged ions are likely produced by step-wise ionization during nanosecond-pulsed laser ablation [21, 50]. During the nanosecond laser beam interaction with the solid target, the leading edge (time) of the laser pulse heats, melts and vaporizes material forming an initial vapor layer above the target surface. The vapor continues to absorb and be ionized by the later part of the ns-laser pulse energy mainly via inverse bremsstrahlung (IB) collisions leading to the plasma formation [8, 51]. If the laser irradiance is high enough, the plasma becomes opaque to the laser radiation before the pulse ending as the electron density increase to a critical value; plasma shielding occurs and absorbs part of the laser energy [52]. With the increase of the absorption of the laser energy during the laser pulse, the atoms and ions in the plasma can be excited and ionized further by the electrons with enough energy via IB mechanism leading to multi-charged ion generation. Plasma shielding effects were investigated and are discussed in the latter part of this manuscript.

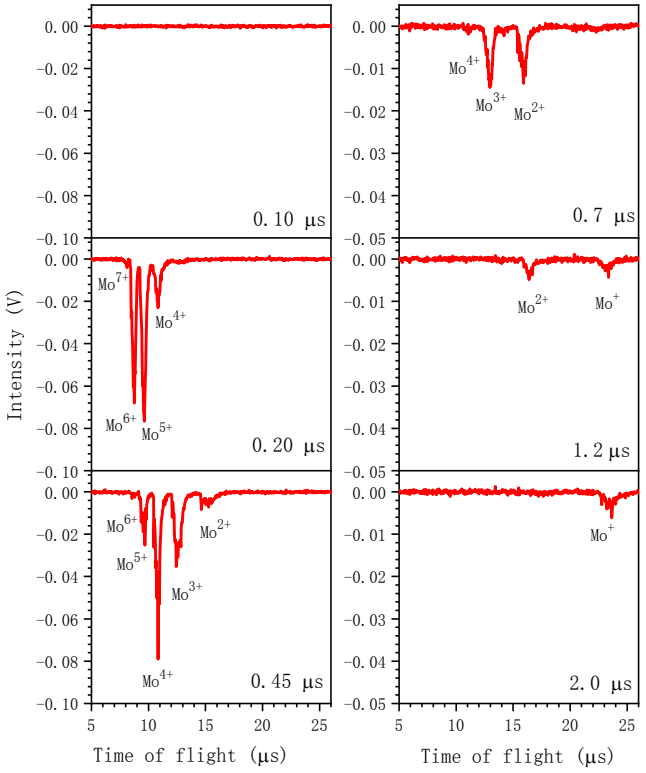

Fig.4 The distribution of Mo^{n+} ions at different delay times with laser power density of 7.9 GW/cm^2.

3.2 Charge state distribution and temporal evolution of Mo ions at different laser power densities

The charge state distribution of the molybdenum ions as a function of the laser power density was investigated (Figure 5). For all mass spectra with the exception of that recorded at laser power density of 0.85 GW/cm^2, the time integration was from 0.1 μs to 2.0 μs. At laser power density of 0.85 GW/cm^2, which is slightly higher than the ablation threshold of the molybdenum target, the plasma plume consists of only a few Mo^+ ions. At laser power density of 1.2 GW/cm^2, Mo^{2+} became predominant as compared to Mo^+. As the laser power density was increased, higher charged-state ions become dominant.

To further elucidate the molybdenum plasma evolution, the temporal behavior of molybdenum ions at these different laser power densities was investigated. The time-resolved TOF-mass spectra of multi-charged ions at different laser power densities were plotted in the false color contour plots shown in Fig.6. For example, the first image shown in Fig.6 corresponds to the specific data presented in Fig.4. The numbers "1+" to "7+" represent the different Mo ion charged states.

As shown in Fig.6, the appearance time (delay time with respect to the laser) of different charged ions were quite different. The observed ion charge state was found to increase with laser power density and the maximum charge state was up to seven at the highest laser power density of 7.9 GW/cm^2. The highest measurable charge state declined with laser power density to a maximum of six at 4.1 GW/cm^2, five at 2.3 GW/cm^2, four at 1.9 GW/cm^2, three at 1.2 GW/cm^2 and only one at 0.85 GW/cm^2. The appearance time of the centroid of each charge state monotonically increased with reducing charge (cf. delay time in Figure 6).

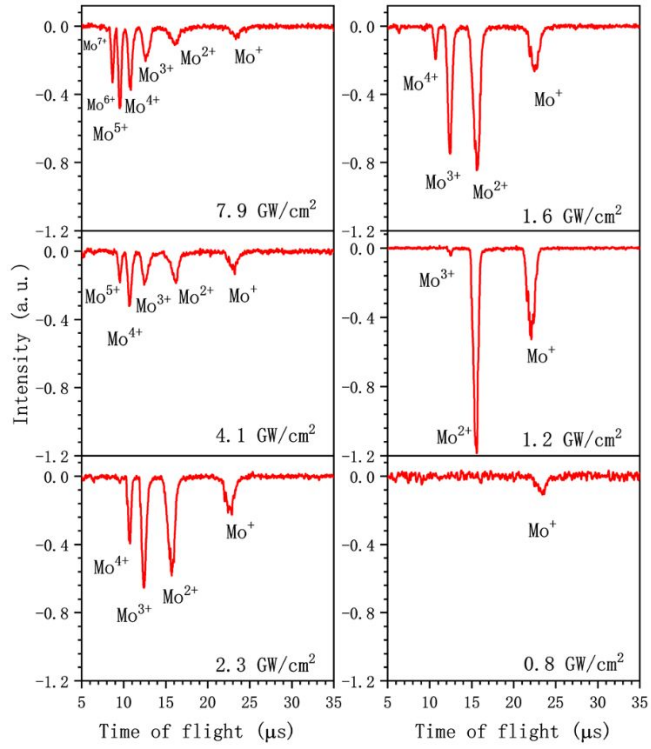

Fig.5 Time-intergrated mass spectra of multi-charged ions at various laser power densities. The integrated time is from 0.1 μs to 2.0 μs for all the mass spectra except the mass spectra at the laser power density of 0.85 W/cm^2.

The last mass spectrum (bottom right) represents time intergration from 0.1 μs to 5 μs.

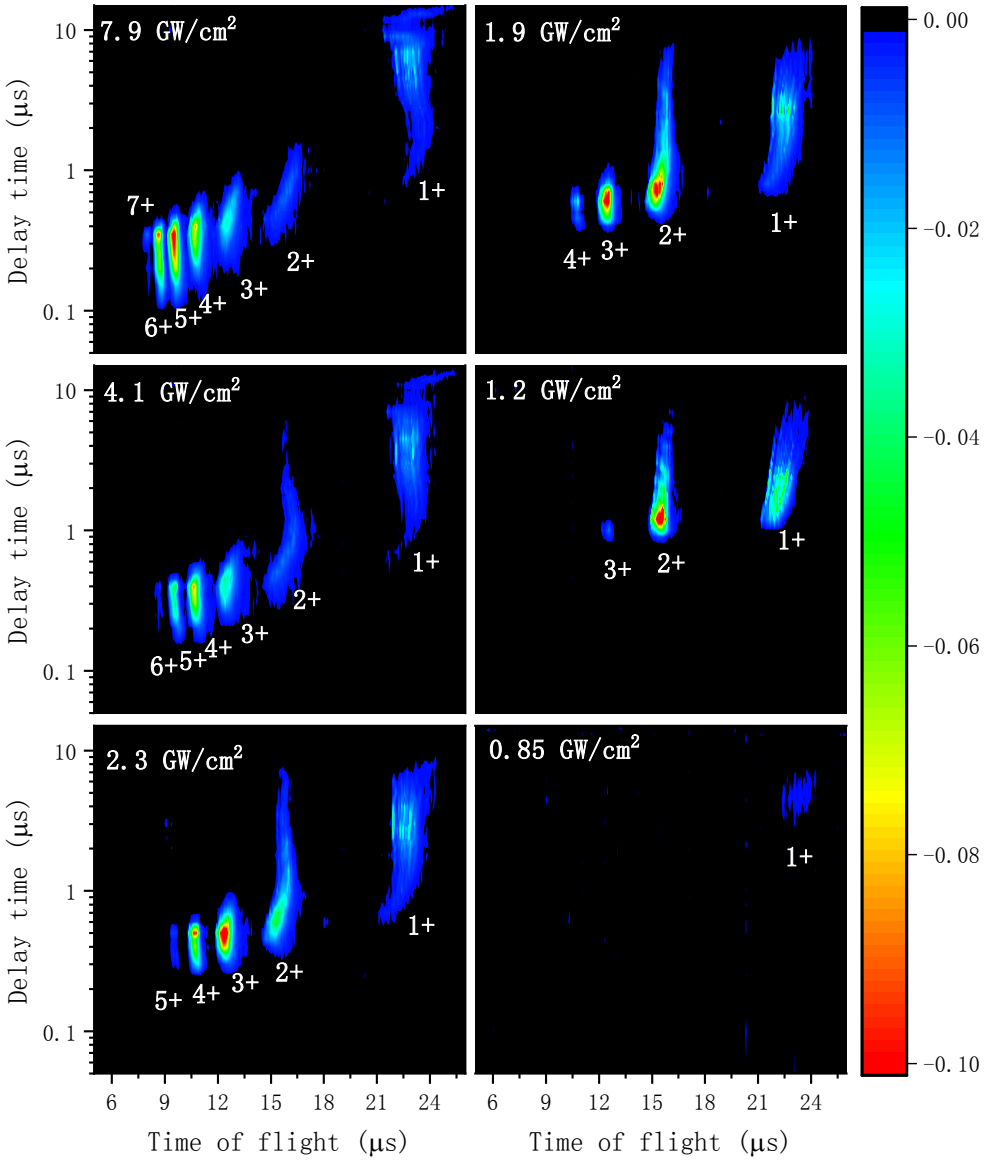

Fig.6 Charge state distribution and temporal evolution of Mo ions at different laser power densities. Numbers from "1+" to "7+" represent the Mo ions of the different charged states.

For example, the temporal evolution of the Mo^{n+} ion intensity at laser power density of 7.9 GW/cm^2 is shown in Fig.7(a). Higher charged ions rose to their peak intensities earlier than the lower charged ions, which shows that separation occurred between these different charged ions during the plasma expansion process. The higher charged ions were found only in the leading edge of the expanding plasma, which means that they travelled with higher velocities. This observation is consistent with previous work on laser produced W and Ta plasmas [43, 53]. In previous work [54-56], the spatial distribution of multi-charged ions of C^{n+}, Si^{n+}, Sn^{n+} in the laser produced plasma was predicted by computer modeling and simulation. From these modeling results in vacuum, higher multi-charged ions was projected to occupy the inner region whereas the lower charged ions and atoms were more concentrated towards the periphery of the laser produced plasma. The predicted results from modeling are opposite from the present experimental findings. This discrepancy could be a result that space charge separation which was not considered in the theoretical models. In the presence of ambient gas, the existence of higher multi-charged ions distributed in the inner region may be true as the collision between the plume-ambient species in the periphery leads to recombination. Moreover, the space charge effect may not be not obvious because of the ambient gas confinement. The duration of the singly charged ions lasts about 10 μs which does not coincide with results obtained using a Faraday cup[57-60]. The typical duration of the ions is estimated about <3 μs at the 2 cm position [60]. The lower velocity of singly charged ion probably is due to the collision at the electrode repellers which confined the lower charged ions, thereby leading to the longer signal duration.

Fig.7 (b) and (c) present the temporal evolution of integrated intensities of Mo^{2+} ions and Mo^{4+} ions, respectively, at representative laser power densities. As the laser power density increased, Mo^{2+} ions and Mo^{4+} ions attained their peak maximum at earlier delay times. In addition, the peak ion intensity of a particular charge state

initially increased with laser power density to a maximum (e.g., the highest ion intensity for Mo^{2+} and Mo^{4+} were found at 1.4 and 4.1 GW/cm^{-2}, respectively), while a further increase in the laser power caused a decline in the intensity of that ion state.

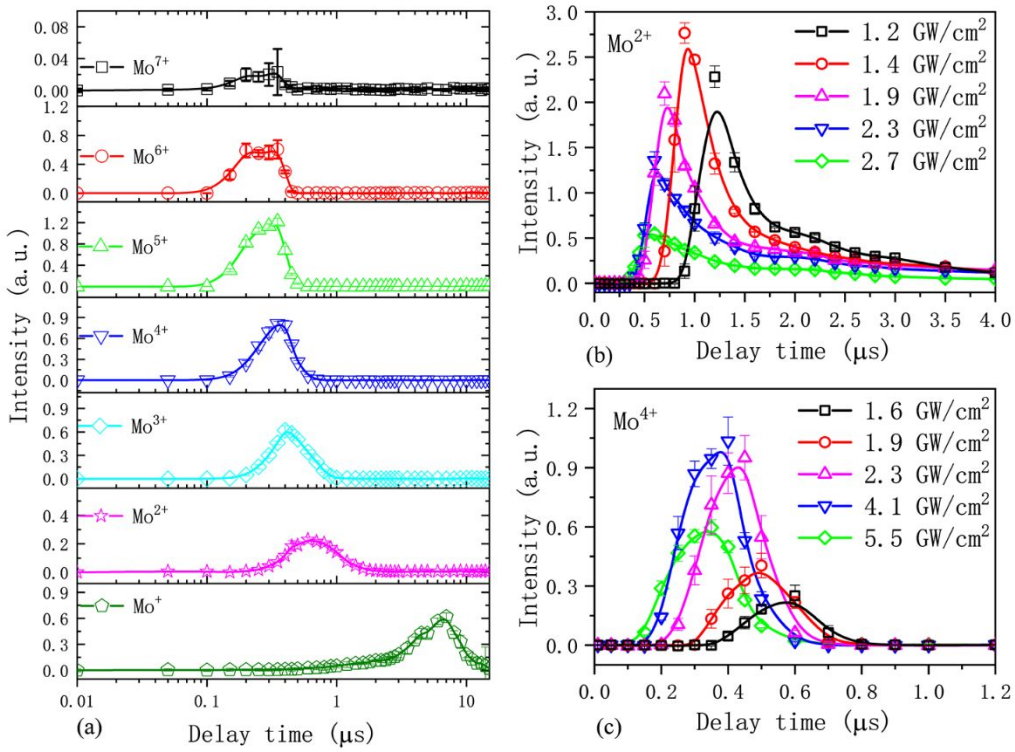

Fig.7 Time evolution of area integrated intensities for the Mo ions at a laser power density of 7.9 GW/cm^2 (a), time evolution of mass spectra intensities of Mo^{2+} ions (b) and Mo^{4+} ions (c) at several laser power densities.

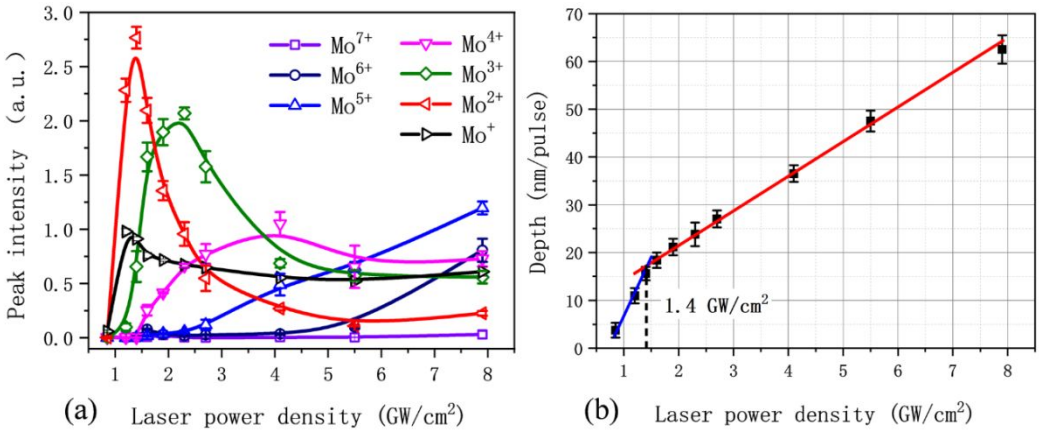

Fig.8 (a) Peak intensities of the different charged ions versus laser power density, (b) the ablation depth versus laser power density. The slope of the line is defined as the ablation rate.

The peak intensities of the different charged ions versus laser power density are shown in Fig.8 (a). The peak intensity values are obtained from the time evolution of mass spectra intensities for the Mo^{n+} ions. From the data shown in Fig.6 and Fig.8 (a), there is a threshold laser power density for each charge state; the charge state can be controlled by the laser power density. This phenomenon also has been reported by Abbasi and Ilyas [21, 50]. Furthermore, it is noted in Fig.8 (a) that after exceeding the optimal laser power density for a particular Mo^{n+} signal, the intensity of Mo^{n+} declined whereas the intensity of $Mo^{(n+1)+}$ ions increased. This observation supports the hypothesis that during the laser ablation process, the $Mo^{(n+1)+}$ ions likely originate from further ionization of the Mo^{n+} ions and multiply charged ions appear to be generated through a step-wise ionization mechanism.

As proposed, multiply-charged ion generation is attributed to plasma shielding. Hence, the reduction of the ablation rate with laser power density increase should occur. Previous studies found that plasma shielding occurs at approximately 0.3 GW/cm^2 with 30 ns pulse duration for laser produced quartz plasma [52]. The plasma shielding threshold for a 5 ns laser pulse is calculated to be approximately 0.5 GW/cm^2 for Cu [61]. The absolute value is dependent on spot size, laser pulse duration, and other parameters.

In order to verify the plasma shielding effect, the laser ablation depth versus laser power density was measured and is shown in Fig.8 (b). It can be seen that plasma shielding occurs at the laser power density of ~1.4 GW/cm^2 where the slope exhibited a transition. This is the laser power density at which multi-charged ions were generated and increased sharply. Hence, plasma shielding seems to play a critical role in multi-charged ion generation.

3.3 Velocity and kinetic energy of - Mo^{n+} ions as a function of laser power density and charge state

The velocity of charged ions was estimated using the vertical distance (2.0 cm) divided by the delay time corresponding to the peak intensity shown in Fig.7(a). Figure 9 (a) and (b) give the velocity of Mo^{n+} ions as a function of laser power density and charge state, respectively. It can be seen that higher charged ions had higher velocities. The maximum velocity observed is up to about 8.0×10^6 m/s.

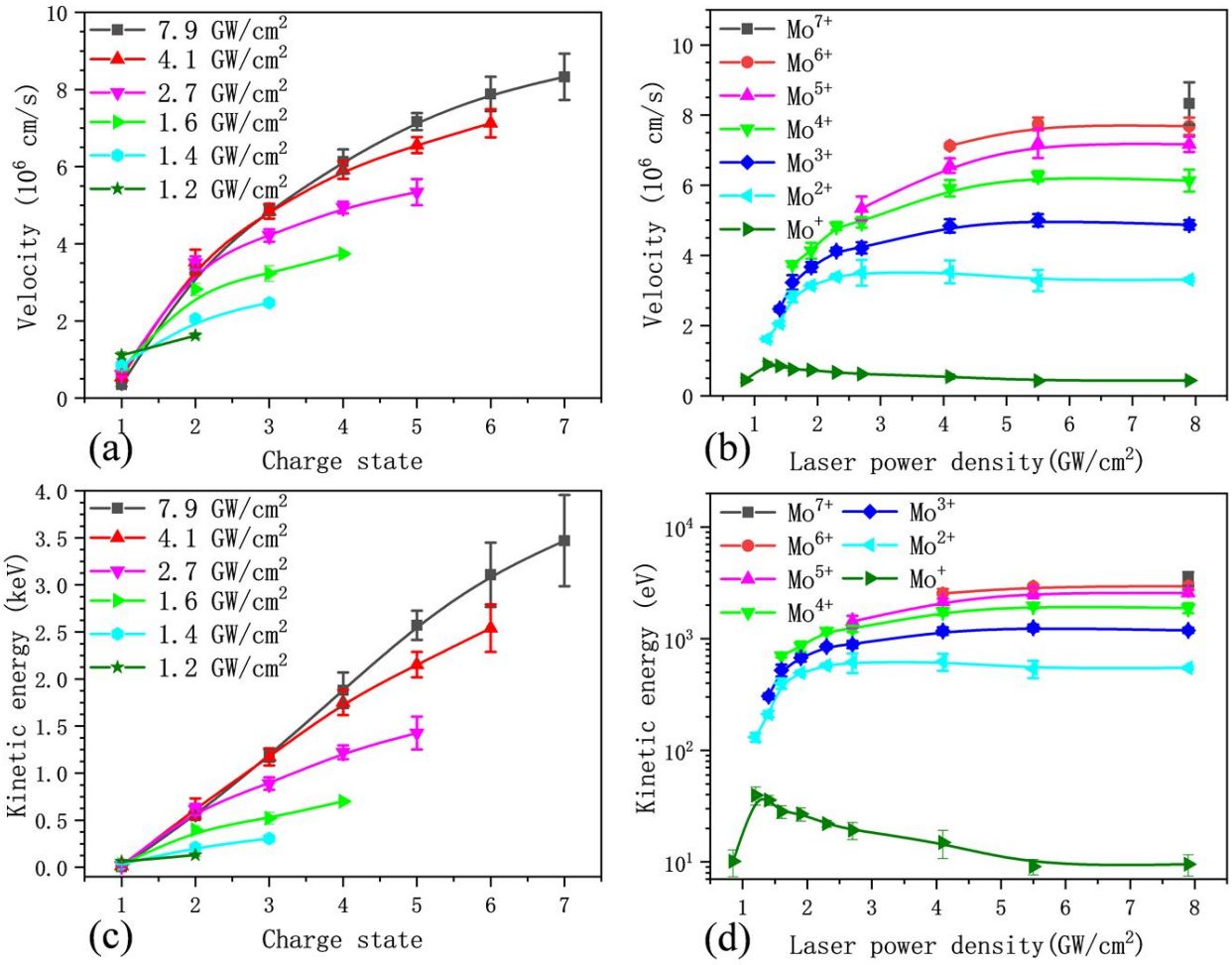

Fig.9 Velocity of Mo^{n+} ions as a fucntion of charge state (a), and laser power density (b). Kinetic energy of Mo^{n+} ions as a fucntion of charge state (c), and laser power density (d).

The acceleration mechanism of ions can be interpreted by transient dynamic sheath acceleration which has been proposed in recent investigations [43] [62]. As discussed earlier, the laser produced plasma is formed primarily by absorbing the ns-laser energy according to inverse bremsstrahlung (IB) heating through electron-ion collisions. The electron-ion thermal equilibration time (10^{-10}–10^{-11} s) [11] is much shorter than the ns-laser pulse duration. Although local thermal equilibrium (LTE) may be valid during the laser interaction process, electron velocities are much faster than those of the ions due to their mass difference. Hence, the electrons would escape from the target surface earlier. As a result, a space charge separation between fast electrons and ions is produced near the target surface and electrons are confined by a self-electric field at the edge of plasma [63, 64]. Some fast electrons may escape, which has been observed in previous work [62, 65], but to maintain electrical neutrality of the plasma as a whole, a substantial fraction of electrons remain at the edge and thus create an electric field with respect to the positively charged core plasma plume, leading to a transient dynamic plasma sheath. The persistence time of the transient plasma sheath is comparable to the laser pulse duration [62, 66, 67]. With the presence of the radial electric field in the plasma sheath, the higher charged ions are accelerated at higher velocities.

As shown in Fig.9 (b) and (d), the velocity or corresponding kinetic energy (1/2 mv^2) for each Mo^{n+} (n>1) ion has a saturation value with the laser power density. The rate of energy increase decreases with power density. In Fig.9 (b) and (d), the inflection point for Mo$^+$ ion is about 1.3 GW/cm^2, the laser power density at which plasma shielding takes place according to the data in Fig.8(b). Hence, the reduction in

the increasing rate of the kinetic energy for the ions could be due to plasma shielding and absorption. It is interesting to note that for Mo^+ ions, the reduction of the energy may be due to more collisions and recombination during the expansion process at higher laser power densities.

4. Conclusion

The dynamic characteristics of multi-charged ion emission from nanosecond laser-induced plasmas on molybdenum targets were investigated using time-of-flight mass spectrometry. The charge state distribution and temporal evolution of multi-charged ions at various laser power densities were systematically studied. The generation of the multi-charged ions is attributed to step-wise ionization due to plasma shielding during the laser plasma interaction. The acceleration mechanisms for the multi-charged ions were attributed to a transient dynamic plasma sheath during the laser interaction process. Energy saturation with the laser power density was observed and the mechanism was discussed. The investigation gives an insight into the physical processes of laser ablation including plasma shielding, multi-charged ions generation and acceleration. Such information is valuable for improvement in laser ablation and plasma expansion modeling, which potentially can lead to better application of LIBS diagnostic studies of the plasma-wall interaction process, as well as better understanding of wall erosion and impurity transportation under extreme conditions like plasma disruptions in tokamaks.

Conflicts of interest

There are no conflicts to declare.

Acknowledgements

This research was supported by the US Department of Energy, Office of Defense Nuclear Nonproliferation Research and Development, under contract number DE-AC02-05CH11231 at the Lawrence Berkeley National Laboratory.

This work also was supported by the National Key R&D Program of China (No.2017YFE0301304), China Postdoctoral Science Foundation (No. 2019M661087), Ding Wu acknowledges the support from the China Scholarship Council (CSC).

References

1. F. jhStock, F. Antoni, L. Diebold, C. C. Gowda, S. Hajjar-Garreau, D. Aubel, N. Boubiche, F. Le Normand and D. Muller, *Applied Surface Science*, 2019, **464**, 562-566.
2. O. Balki, M. M. Rahman and H. E. Elsayed-Ali, *Optics Communications*, 2018, **412**, 134-140.
3. A. McBain, V. Vuppuluri, I. E. Gunduz, L. J. Groven and S. F. Son, *Combustion and Flame*, 2018, **188**, 104-115.
4. L. Jiao, B. S. Truscott, H. Liu, M. N. R. Ashfold and H. H. Ma, *Journal of Applied Physics*, 2017, **121**, 013303.
5. S. Atzeni, J. Meyer-Ter-Vehn and J. Meyer-ter-Vehn, *The Physics of Inertial Fusion: BeamPlasma Interaction, Hydrodynamics, Hot Dense Matter*, Oxford University Press on Demand, 2004.
6. C. Wagner and N. Harned, *Nature Photonics*, 2010, **4**, 24-26.
7. C. S. Musgrave, T. Murakami, T. Ugomori, K. Yoshida, S. Fujioka, H. Nishimura, H. Atarashi, T. Iyoda and K. Nagai, *Rev Sci Instrum*, 2017, **88**, 033506.
8. S. Musazzi and U. Perini, *Springer Series in Optical Sciences*, 2014, **182**.
9. A. A. Bol'shakov, X. Mao, J. J. González and R. E. Russo, *Journal of Analytical Atomic Spectrometry*, 2016, **31**, 119-134.
10. R. E. Russo, A. A. Bol'shakov, X. Mao, C. P. McKay, D. L. Perry and O. Sorkhabi, *Spectrochimica Acta Part B: Atomic Spectroscopy*, 2011, **66**, 99-104.
11. D. Marla, U. V. Bhandarkar and S. S. Joshi, *Journal of Applied Physics*, 2011, **109**, 021101.
12. J. S. Becker, M. Zoriy, A. Matusch, B. Wu, D. Salber, C. Palm and J. S. Becker, *Mass spectrometry reviews*, 2010, **29**, 156-175.
13. M. R. Dong, D. Oropeza, J. Chirinos, J. J. Gonzalez, J. D. Lu, X. L. Mao and R. E. Russo, *Spectroc. Acta Pt. B-Atom. Spectr.*, 2015, **109**, 44-50.
14. G. G. Gladush and I. Smurov, *Physics of laser materials processing: theory and experiment*, Springer Science & Business Media, 2011.
15. M. Stafe, A. Marcu and N. N. Puscas, *Pulsed laser ablation of solids: basics, theory and applications*, Springer Science & Business Media, 2013.
16. P.-E. Nica, S. A. Irimiciuc, M. Agop, S. Gurlui, M. Ziskind and C. Focsa, 2017, DOI: 10.5772/intechopen.70759.
17. B. Verhoff, S. S. Harilal, J. R. Freeman, P. K. Diwakar and A. Hassanein, *Journal of Applied Physics*, 2012, **112**, 093303.
18. F. Trichard, S. Moncayo, D. Devismes, F. Pelascini, J. Maurelli, A. Feugier, C. Sasseville, F. Surma and V. Motto-Ros, *Journal of Analytical Atomic Spectrometry*, 2017, **32**, 1527-1534.
19. P. Veis, A. Marín-Roldán and J. Krištof, *Plasma Sources Science and Technology*, 2018, **27**, 095001.
20. M. J. Padgett, J. Stuhler, A. J. Shields, P. Hayden, P. Nicolosi, J. Costello and S. S. Zehra, 2018, DOI:

10.1117/12.2306459, 53.
21. B. Ilyas, A. H. Dogar, S. Ullah, N. Mahmood and A. Qayyum, *Laser and Particle Beams*, 2012, **30**, 651-657.
22. S. Abbasi, A. Dogar, B. Ilyas, S. Ullah, M. Rafique and A. Qayyum, *Laser and Particle Beams*, 2016, **34**, 606-614.
23. M. H. A. Shaim and H. E. Elsayed-Ali, *Journal of Applied Physics*, 2017, **122**, 203301.
24. R. A. Burdt, Y. Tao, M. S. Tillack, S. Yuspeh, N. M. Shaikh, E. Flaxer and F. Najmabadi, *Journal of Applied Physics*, 2010, **107**, 043303.
25. Z. H. Hu, N. Gierse, C. Li, J. Oelmann, D. Y. Zhao, M. Tokar, X. Jiang, D. Nicolai, J. Wu, F. Ding, S. Brezinsek, H. B. Ding, G. N. Luo and C. Linsmeier, *Fusion Engineering and Design*, 2018, **135**, 95-101.
26. D. Zhao, C. Li, Z. Hu, C. Feng, Q. Xiao, R. Hai, P. Liu, L. Sun, D. Wu, C. Fu, J. Liu, N. Farid, F. Ding, G. N. Luo, L. Wang and H. Ding, *Rev Sci Instrum*, 2018, **89**, 073501.
27. C. Li, N. Gierse, J. Oelmann, S. Brezinsek, M. Rasinski, C. P. Dhard, T. S. Pedersen, R. Konig, Y. F. Liang, H. Ding, C. Linsmeier and W.-X. team, *Physica Scripta*, 2017, **T170**, 014004.
28. Z. Hu, N. Gierse, C. Li, P. Liu, D. Zhao, L. Sun, J. Oelmann, D. Nicolai, D. Wu, J. Wu, H. Mao, F. Ding, S. Brezinsek, Y. Liang, H. Ding, G. Luo and C. Linsmeier, *Physica Scripta*, 2017, **T170**, 014046.
29. N. Gierse, B. Schweer, A. Huber, O. Karger, V. Philipps, U. Samm and G. Sergienko, *Journal of Nuclear Materials*, 2011, **415**, S1195-S1198.
30. N. Gierse, M. Z. Tokar, S. Brezinsek, T. F. Giesen, M. Hubeny, A. Huber, V. Philipps, A. Pospieszczyk, G. Sergienko, J. Wegner, Q. Xiao, U. Samm, C. Linsmeier and T. Team, *Physica Scripta*, 2016, **T167**.
31. N. Gierse, S. Brezinsek, J. W. Coenen, T. F. Giesen, A. Huber, M. Laengner, S. Moller, M. Nonhoff, V. Philipps, A. Pospieszczyk, B. Schweer, G. Sergienko, Q. Xiao, M. Zlobinski, U. Samm and T. Team, *Physica Scripta*, 2014, **T159**.
32. J. Dong, L. Liang, J. Wei, H. Tang, T. Zhang, X. Yang, K. Wang and H. Li, *Journal of Analytical Atomic Spectrometry*, 2015, **30**, 1336-1344.
33. T. Takahashi, B. Thornton, K. Ohki and T. Sakka, *Spectrochimica Acta Part B: Atomic Spectroscopy*, 2015, **111**, 8-14.
34. G. S. Maurya, R. Kumar, A. Kumar and A. K. Rai, *Spectroc. Acta Pt. B-Atom. Spectr.*, 2016, **126**, 17-22.
35. C.-T. Chen, D. Banaru, T. Sarnet and J. Hermann, *Spectrochimica Acta Part B: Atomic Spectroscopy*, 2018, **150**, 77-85.
36. C. L. Fu, Q. Wang and H. B. Ding, *Plasma Science & Technology*, 2018, **20**.
37. I. Gornushkin, T. Völker and A. Y. Kazakov, *Spectrochimica Acta Part B: Atomic Spectroscopy*, 2018, **147**, 149-163.
38. R. Fantoni, S. Almaviva, L. Caneve, F. Colao, A. M. Popov and G. Maddaluno, *Spectroc. Acta Pt. B-Atom. Spectr.*, 2013, **87**, 153-160.
39. R. Fantoni, S. Almaviva, L. Caneve, F. Colao, G. Maddaluno, P. Gasior and M. Kubkowska, *Spectroc. Acta Pt. B-Atom. Spectr.*, 2017, **129**, 8-13.
40. S. Almaviva, L. Caneve, F. Colao, P. Gasior, M. Kubkowska, M. Lepek and G. Maddaluno, *Fusion Engineering and Design*, 2015, **96-97**, 848-851.
41. A. M. Elsied, P. K. Diwakar, M. Polek and A. Hassanein, *Journal of Applied Physics*, 2016, **120**, 173104.
42. D. Y. Zhao, C. Li, Y. Wang, Z. W. Wang, L. Gao, Z. H. Hu, J. Wu, G. N. Luo and H. B. Ding, *Plasma Science & Technology*, 2018, **20**, 8.
43. D. Wu, L. Zhang, P. Liu, L. Sun, R. Hai and H. Ding, *Spectrochimica Acta Part B: Atomic Spectroscopy*, 2017, **137**, 70-76.
44. Y. Ralchenko, *Memorie della Societa Astronomica Italiana Supplementi*, 2005, **8**, 96.
45. Z. Liu, X. Gao, S. Liu, S. Ding, T. Xia, T. Zhang, S. Zhang, Y. Wang, X. Han and J. Li, *Nuclear Fusion*, 2013, **53**, 073041.
46. U. Boesl, *Mass spectrometry reviews*, 2017, **36**, 86-109.
47. T. W. Suen, UC Berkeley, 2012.
48. A. Thum-Jager and K. Rohr, *Journal of Physics D: Applied Physics*, 1999, **32**, 2827-2831.
49. A. Thum-Jaeger, B. K. Sinha and K. P. Rohr, *Phys Rev E Stat Nonlin Soft Matter Phys*, 2001, **63**, 016405.
50. S. Abbasi, M. Hussain, B. Ilyas, M. Rafique, A. Dogar and A. Qayyum, *Laser and Particle Beams*, 2015, **33**, 81-86.
51. F. Caridi, L. Torrisi, D. Margarone and A. Borrielli, *Laser and Particle Beams*, 2008, **26**, 265-271.
52. X. Mao and R. E. Russo, *Applied Physics A*, 1996, **64**, 1-6.
53. L. Torrisi, S. Gammino, L. Andò and L. Làska, *Journal of Applied Physics*, 2002, **91**, 4685-4692.
54. Q. Min, M. Su, S. Cao, D. Sun, G. O'Sullivan and C. Dong, *Opt Lett*, 2016, **41**, 5282-5285.
55. M. G. Su, Q. Min, S. Q. Cao, D. X. Sun, P. Hayden,

G. O'Sullivan and C. Z. Dong, *Sci Rep*, 2017, **7**, 45212.
56. Q. Min, M. Su, S. Cao, D. Sun, G. O'Sullivan and C. Dong, *Opt Express*, 2018, **26**, 7176-7189.
57. A. H. Dogar, S. Ullah, H. Qayyum, Z. U. Rehman and A. Qayyum, *Journal of Physics D-Applied Physics*, 2017, **50**, 385602.
58. M. Comet, M. Versteegen, F. Gobet, D. Denis-Petit, F. Hannachi, V. Meot and M. Tarisien, *Journal of Applied Physics*, 2016, **119**, 013301.
59. A. M. Elsied, P. K. Diwakar, M. Polek and A. Hassanein, *Journal of Applied Physics*, 2016, **120**, 173104.
60. B. Ilyas, A. H. Dogar and A. Qayyum, *Nuclear Instruments & Methods in Physics Research Section B-Beam Interactions with Materials and Atoms*, 2013, **312**, 122-125.
61. A. Bogaerts and Z. Y. Chen, *Spectroc. Acta Pt. B-Atom. Spectr.*, 2005, **60**, 1280-1307.
62. D. Wu, L. Y. Sun, J. M. Liu, X. Yu, R. Hai, C. L. Feng, Z. W. Wang and H. B. Ding, *Physics of Plasmas*, 2019, **26**.
63. S. S. Mao, X. Mao, R. Greif and R. E. Russo, *Applied Physics Letters*, 2000, **77**, 2464-2466.
64. S. S. Mao, X. Mao, R. Greif and R. E. Russo, *Applied Physics Letters*, 2000, **76**, 31-33.
65. N. Farid, S. S. Harilal, H. Ding and A. Hassanein, *Physics of Plasmas*, 2013, **20**, 073114.
66. L. Torrisi, F. Caridi, D. Margarone and A. Borrielli, *Applied Surface Science*, 2008, **254**, 2090-2095.
67. L. Torrisi, F. Caridi and L. Giuffrida, *Laser and Particle Beams*, 2011, **29**, 29-37.

The charge state distribution and temporal evolution of the laser-produced molybdenum plasma were investigated at various laser power densities.